New Journal of Physics
The open–access journal for physics

A de Haas–van Alphen study of the filled skutterudite compounds $PrOs_4As_{12}$ and $LaOs_4As_{12}$

Pei-Chun Ho[1], J Singleton[2,6], M B Maple[1], Hisatomo Harima[3], P A Goddard[2,4], Z Henkie[5] and A Pietraszko[5]

[1] Department of Physics and Institute for Pure and Applied Physical Sciences, University of California, San Diego, 9500 Gilman Drive, Dept 0360, La Jolla, CA 92093-0360, USA
[2] National High Magnetic Field Laboratory, Los Alamos National Laboratory, MS-E536, Los Alamos, NM 87545, USA
[3] Department of Physics, Kobe University, 1-1 Rokko-dai Noda Kobe 657-8501, Japan
[4] Clarendon Laboratory, Oxford University, Parks Road, Oxford OX1 3PU, UK
[5] Institute for Low Temperature and Structure Research, Polish Academy of Sciences, 50-950, Wroclaw, Poland
E-mail: jsingle@lanl.gov

New Journal of Physics **9** (2007) 269
Received 18 May 2007
Published 15 August 2007
Online at http://www.njp.org/
doi:10.1088/1367-2630/9/8/269

Abstract. Comprehensive magnetic-field-orientation dependent studies of the susceptibility and de Haas–van Alphen effect have been carried out on single crystals of the filled skutterudites $PrOs_4As_{12}$ and $LaOs_4As_{12}$ using magnetic fields of up to 40 T. Several peaks are observed in the low-field susceptibility of $PrOs_4As_{12}$, corresponding to cascades of metamagnetic transitions separating the low-field antiferromagnetic and high-field paramagnetic metal (PMM) phases. The de Haas–van Alphen experiments show that the Fermi-surface topologies of $PrOs_4As_{12}$ in its PMM phase and $LaOs_4As_{12}$ are very similar. In addition, they are in reasonable agreement with the predictions of bandstructure calculations for $LaOs_4As_{12}$ on the $PrOs_4As_{12}$ lattice. Both observations suggest that the Pr 4f electrons contribute little to the number of itinerant quasiparticles in the PMM phase. However, while the properties of $LaOs_4As_{12}$ suggest a conventional nonmagnetic Fermi liquid, the effects of direct exchange and electron correlations are detected in the PMM phase of $PrOs_4As_{12}$. For example, the

[6] Author to whom any correspondence should be addressed.

PII: S1367-2630(07)50805-0

quasiparticle effective masses in $PrOs_4As_{12}$ are found to decrease with increasing field, probably reflecting the gradual suppression of magnetic fluctuations associated with proximity to the low-temperature, low-field antiferromagnetic state.

Contents

1. Introduction

Filled skutterudite compounds, with the formula MT_4X_{12}, where M is an alkali metal, alkaline-earth, lanthanide or actinide, T is Fe, Ru or Os and X is P, As or Sb, display a wide range of interesting phenomena caused by strong electron correlations [1]–[3]. The case M = Pr has attracted particular interest, where it is thought that many of the physical properties are attributable to the ground state and the low-lying excited state of the Pr^{3+} ion in the crystalline electric field (CEF), and the hybridization of the Pr 4f orbitals with the ligand states of the surrounding ionic cage [4]–[9]. A variety of correlated-electron phenomena have been observed in the Pr-based filled skutterudites: conventional Bardeen–Cooper–Schrieffer (BCS) and unconventional superconductivity, magnetic order, quadrupolar order, metal-insulator transitions, Kondo phenomena, heavy-fermion behavior and non-Fermi-liquid behavior [1, 2], [4]–[7], [9]–[11].

Much of this work has been carried out on the filled-skutterudite phosphides and antimonides; by contrast, arsenides have not been investigated in as much detail. However, initial measurements of $PrOs_4As_{12}$ [12, 13] show that it exhibits interesting low-temperature properties that are a consequence of strong electron correlations, making it worthy of further careful study. $PrOs_4As_{12}$ enters an antiferromagnetic state at low temperatures; this phase possesses a greatly enhanced electronic specific heat coefficient $\gamma \approx 1\,\mathrm{J\,mol^{-1}\,K^{-2}}$, highly suggestive of heavy-fermion behavior [12]. On applying magnetic fields $\mu_0 H \approx 3$–$4\,\mathrm{T}$, the antiferromagnetic phase is destroyed and the value of γ collapses as $PrOs_4As_{12}$ enters what is believed to be a paramagnetic-metal phase PMM [13]. In this paper, we present an investigation of the de Haas–van Alphen effect and susceptibility in $PrOs_4As_{12}$ single crystals. Corresponding experiments were also carried out on crystals of the isostructural nonmagnetic metal $LaOs_4As_{12}$.

Our susceptibility measurements show that the antiferromagnetic to PMM transition in $PrOs_4As_{12}$ in fact proceeds via 3 or 4 metamagnetic transitions, the field positions of which depend strongly on the orientation of the crystal in the field. The de Haas–van Alphen experiments demonstrate that the Fermi-surface topologies of $PrOs_4As_{12}$ in its PMM phase and $LaOs_4As_{12}$ are rather similar. However, whereas $LaOs_4As_{12}$ behaves as a fairly conventional low-effective-mass Fermi liquid, we find that the PMM phase of $PrOs_4As_{12}$ exhibits the effects of a direct exchange coupling and shows quasiparticle effective masses that are renormalized by fluctuations associated with the proximity of the low-field, low-temperature antiferromagnetic state.

2. Experimental details and bandstructure calculations

Single crystals of $PrOs_4As_{12}$ and $LaOs_4As_{12}$ were grown from elements with purities 99.9% using the high-temperature molten-metal-flux procedure described in [12]. As-grown crystals were cleaned in acid to remove residual flux and impurity phases from their surfaces. The crystals (cubic space group Im $\bar{3}$; for structural details see [12, 13]) are truncated octahedra (8 large {111} faces and 6, approximately square, smaller {100} faces), with largest dimensions in the range 0.1–1 mm; the presence of well-defined crystal faces greatly aids the accurate orientation of the samples in the magnetic field.

The measurements carried out in quasistatic magnetic fields employ a torque magnetometer with a cantilever constructed from 5 μm phosphor bronze[7]. A single crystal is glued to the cantilever via a thin sheet of strain-reducing paper. The interaction between the sample's magnetic moment $\mathbf{m}$ and the applied magnetic field $\mathbf{B}$ causes a torque $-\mathbf{m} \times \mathbf{B}$ that results in a deflection of the cantilever. The deflection is monitored using the capacitance between the cantilever and a fixed plate about 1 mm below it ($\sim$0.5 pF), measured using a General Radio capacitance bridge. Care is taken to ensure that deflections are small, so that the sample's orientation in the field is not changed significantly by the torque. The torque magnetometer is mounted on a two-axis cryogenic goniometer that allows the sample orientation to be changed *in situ*; ^{3}He refrigeration provides temperatures in the range 0.45–10 K. Quasistatic magnetic fields were provided by a superconducting magnet in Los Alamos and by 33 T Bitter coils at the National High Magnetic Field Laboratory (NHMFL) Tallahassee.

Pulsed-field experiments use a 1 mm bore, 1 mm long compensated-coil susceptometer, constructed from 50-gauge high-purity copper wire. The coil is wound with approximately 640 turns in one sense, followed by around 360 in the opposite sense; final turns are added or subtracted by hand on the bench-top to reduce the uncompensated area of the coil to a fraction of a turn. Fine-tuning of the compensation is accomplished by electronically adding or subtracting a small part of the voltage induced in a coaxial single-turn coil wound around the susceptometer [15]. Once this has been done, the signal from the susceptometer is $V \propto (\mathrm{d}M/\mathrm{d}t) = (\mathrm{d}M/\mathrm{d}H)(\mathrm{d}H/\mathrm{d}t)$, where M is the magnetization of a sample placed within the bore of the coil and H is the applied magnetic field [15]. Magnetic fields were provided by the 40 T mid-pulse magnet at NHMFL Los Alamos (see [16] and references therein); the use of this magnet, with its relatively slow rise time ($\approx$100 ms) was necessary to avoid inductive sample heating. The susceptometer was placed within a simple ^{3}He cryostat providing temperatures down to 0.4 K. Magnetic fields were deduced by integrating the voltage induced in an

[7] The principles are similar to those of the device described in [14].

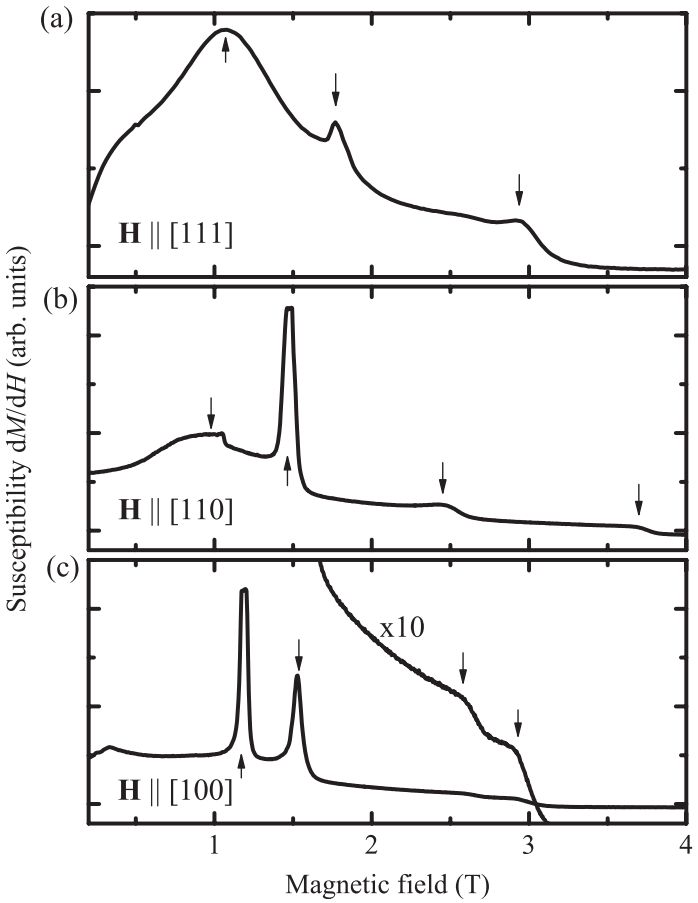

Figure 1. (a) Differential susceptibility (dM/dH) of a single crystal of $PrOs_4As_{12}$ for $\mathbf{H} \parallel [111]$ ($T = 0.57$ K). Three metamagnetic transitions are observed as peaks, indicated by arrows. It is possible that a fourth transition occurs at about 2.6 T. (b) Similar susceptibility data for $\mathbf{H} \parallel [110]$ ($T = 0.51$ K); four metamagnetic transitions may be seen (arrows). (c) Susceptibility data for $\mathbf{H} \parallel [100]$ ($T = 0.51$ K); the data between 2 and 3 T have been multiplied by 10 to enhance the visibility of features. Four metamagnetic transitions may be seen (arrows).

eleven-turn coil, calibrated by observing the de Haas–van Alphen oscillations of the belly orbits of the copper coils of the susceptometer [15].

The bandstructure of $PrOs_4As_{12}$ was calculated using a full-potential linearized augmented plane wave (FLAPW) and local density approximation (LDA) method (for further details see [8, 17, 18]). The 4f electrons are assumed to be localized, so that the calculation is essentially for $LaOs_4As_{12}$ on the $PrOs_4As_{12}$ lattice.

3. Low-field susceptibility and phase diagram

Figure 1 shows the low-field susceptibility (dM/dH) of a single crystal of $PrOs_4As_{12}$, measured using the pulsed-field susceptometer, for three different orientations of the sample in the

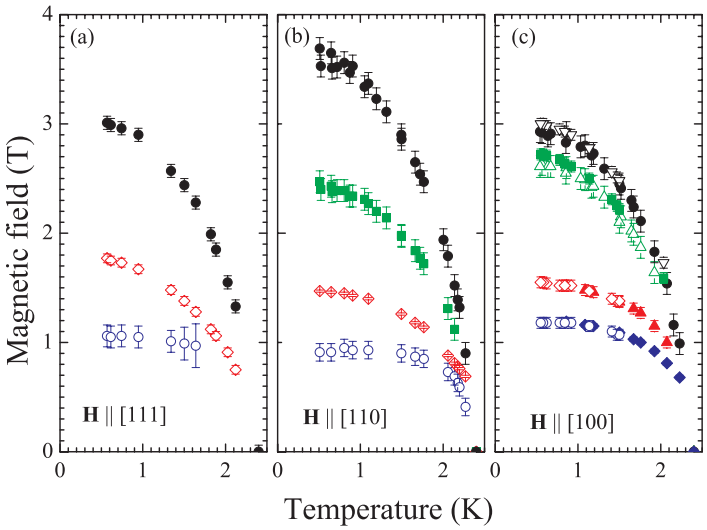

Figure 2. H, T phase diagrams of the peaks in the susceptibility of $PrOs_4As_{12}$ for (a) **H** ∥ [111] (b) **H** ∥ [110] and (c) **H** ∥ [100]. Data for samples from two different batches are shown in (c) (indicated by filled and hollow symbols), indicating that the peak positions are an intrinsic feature of the material. The transitions surround the low-field, low-temperature antiferromagnetic phase [13]; the region outside the transitions is the PMM phase.

magnetic field. Previous heat-capacity experiments for **H** ∥ [111] [12, 13] have suggested that two field-induced phase transitions occur in $PrOs_4As_{12}$ at low temperatures. However, in the present experiments, at each orientation, three or four peaks (or humps) are observed in (dM/dH), corresponding to metamagnetic transitions involving a broadened, step-like change in M (see e.g. [19]). The (H, T) positions of the transitions are plotted in figure 2; the $H = 0$ point is $T \approx 2.4$ K, a temperature above which there is definitely no discernable trace of features in the low-field susceptibility. This is close to the zero-field Néel temperatures $T_N = 2.28$ and 2.5 K inferred respectively from neutron-scattering and conventional magnetometry experiments on $PrOs_4As_{12}$ [13]. This suggests that the low-field antiferromagnetic phase is a prerequisite for the transitions seen in the susceptibility. The fact that the transitions are closely spaced and occur at fields that change rather slowly with changing temperature may be the reason why fewer features have been detected in fixed-field, swept temperature experiments [13].

By contrast, apart from a feature attributable to the superconducting critical field [20], the low-field susceptibility of $LaOs_4As_{12}$ was free of metamagnetic transitions, as might be expected for what is thought to be a relatively conventional, nonmagnetic Fermi liquid [20].

4. de Haas–van Alphen effect

4.1. Frequency spectrum and the effects of direct exchange

At fields above those shown in figures 1 and 2 (i.e. in the PMM phase of $PrOs_4As_{12}$), the low-temperature responses of the torque magnetometer and pulsed-field susceptometer become dominated by de Haas–van Alphen oscillations. Oscillations in the torque are shown

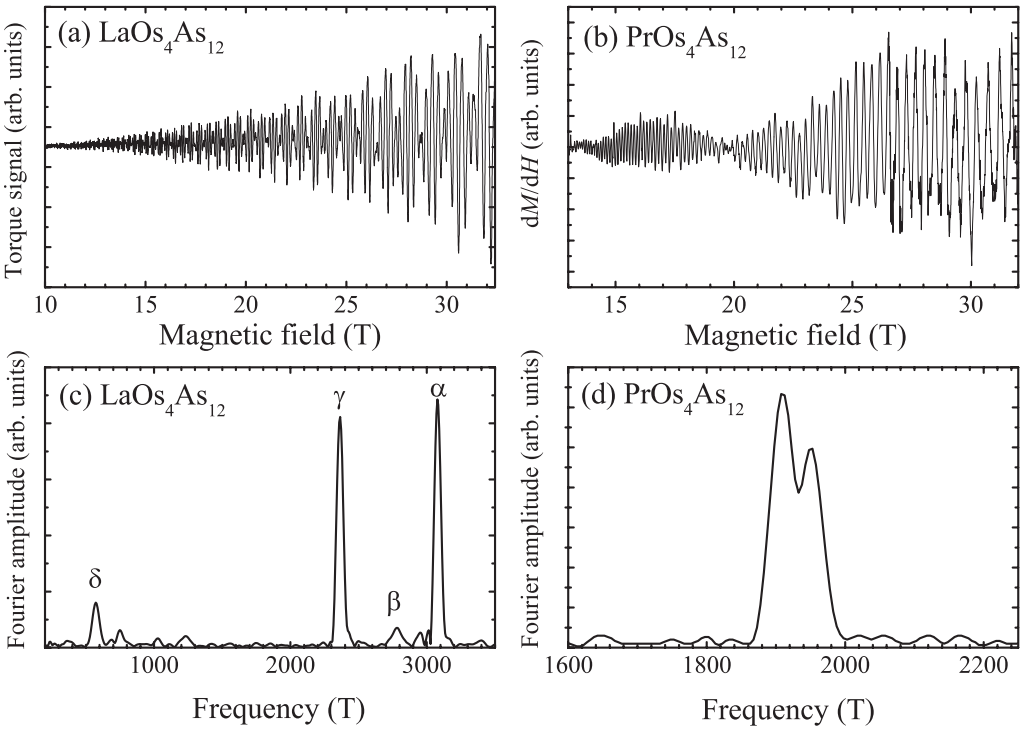

Figure 3. (a) de Haas–van Alphen oscillations in the torque magnetometer signal for $LaOs_4As_{12}$ ($T = 1.0$ K). The quantity plotted is the change in capacitance of the magnetometer, proportional to the torque for small deflections [14]. The sample has been tilted about the $[1\bar{1}0]$ axis so that its [100] direction makes an angle of $\theta = 15.3^\circ$ with the magnetic field. (b) Pulsed-field susceptometer data for $PrOs_4As_{12}$ (0.52 K, field parallel to [110]). The quantity plotted is the voltage induced in the susceptometer coil divided by dH/dt; it is proportional to dM/dH (see section 2). The de Haas–van Alphen oscillations show a node at 20 T due to the beating of two closely-spaced frequencies caused by direct exchange splitting of the Fermi surface into spin-up and spin-down components (see (d) below). (c) Fourier transform of the $LaOs_4As_{12}$ data in (a), showing four de Haas–van Alphen frequencies, labeled α–δ. (d) Expansion of a Fourier transform of $PrOs_4As_{12}$ de Haas–van Alphen oscillations (pulsed-field susceptometer) close to the γ frequency. The field is parallel to [110], the temperature is 0.52 K and a field window of 12–30 T was used for the transform in order to attain a high resolution. Under such conditions it can be seen that the γ peak is split; i.e. the γ oscillations in $PrOs_4As_{12}$ in fact comprise two closely-spaced frequencies γ_1 and γ_2. A similar splitting is seen for the α, β and δ frequencies. It is the presence of both γ_1 and γ_2 frequencies that lead to the node seen in (b).

in figure 3(a) for $LaOs_4As_{12}$, and an example of oscillations in pulsed-field susceptometer data is given in figure 3(b) for $PrOs_4As_{12}$. The complex form of the oscillations suggests the presence of several de Haas–van Alphen frequencies, each corresponding, via the Onsager relationship, to different Fermi-surface cross-sections in the plane perpendicular to the magnetic field [21]. Numerical Fourier transformation was used to extract the frequencies of the oscillations

(figures 3(c) and (d)). Once obvious higher harmonics are accounted for in the Fourier transforms, four de Haas–van Alphen frequencies are consistently observable in $PrOs_4As_{12}$ and $LaOs_4As_{12}$ (figure 3(c)), corresponding to four Fermi-surface sections (FSSs). Following the precedents set by de Haas–van Alphen studies of other filled skutterudites [7, 8, 22], we label the FSSs (frequencies) using the Greek letters α–δ, with α corresponding to the largest orbit (figure 3(c)).

Although the frequencies observed in $PrOs_4As_{12}$ and $LaOs_4As_{12}$ are similar, an interesting difference between the materials is visible if a large enough field window (i.e. high enough resolution [21]) is used for the Fourier transform of the data. Whereas in $LaOs_4As_{12}$ each of the peaks α–δ in Fourier amplitude (figure 3(c)) corresponds to a single frequency, those in $PrOs_4As_{12}$ each comprise a pair of closely-spaced frequencies (figure 3(d)). These very similar frequencies cause a beating in the de Haas–van Alphen signal, resulting in observable nodes; an example is shown in figure 3(b). Some illustrative values of the splitting are given in table 1.

The presence of pairs of closely-spaced frequencies suggests that each of the FSSs in $PrOs_4As_{12}$ is split into spin-up and spin-down components by direct exchange coupling, as befits a polarized, strongly PMM [23]. The exchange interactions act as an effective field that results in populations of spin-up and spin-down quasiparticles that are no longer equal. Thus, the Fermi-surface cross-sections differ for spin-up and spin-down quasiparticles, resulting in the observed splitting of each de Haas–van Alphen frequency into two closely-spaced components. This effect has been noted in a number of magnetic hexaborides (see [23] and citations therein). Later in the paper, we shall use the frequency splitting and other data to estimate the exchange coupling in the paramagnetic phase of $PrOs_4As_{12}$.

4.2. Three-dimensional Fermi-surface topology

The Fermi surface of $PrOs_4As_{12}$ predicted by the LDA/FLAPW calculations is shown in figure 4. In order to check this three-dimensional picture of the Fermi-surface, torque magnetometry data sets were recorded at ^{3}He base temperature for both $PrOs_4As_{12}$ and $LaOs_4As_{12}$ at several orientations of the magnetic field, using the cryogenic goniometer to rotate the sample. A disadvantage of torque magnetometry is that the signal is very small or absent when the field is exactly aligned along a symmetry direction of the crystal; hence, additional data were recorded with the field along the [111], [110] and [100] directions using the pulsed-field susceptometer. Both techniques are in good agreement.

The frequencies are shown for $PrOs_4As_{12}$ (PMM phase) as a function of field orientation in figure 5(a) and for $LaOs_4As_{12}$ in figure 5(b). The orientation dependences of the observable frequencies suggest that the Fermi surfaces of both materials are rather similar.

In addition, the de Haas–van Alphen frequencies predicted for the calculated Fermi surface of figure 4 are shown in figure 5(a). Frequencies α–δ are seen to correspond to the main extremal orbits about the calculated FSSs (bold lines in figure 4)[8]. The strong qualitative similarity between the theoretical de Haas–van Alphen frequencies and the experimental data (figure 5(a)) suggest that the Pr ions make little contribution to the itinerant quasiparticles in the PMM phase of $PrOs_4As_{12}$; the LDA/FLAPW calculations assume localized 4f electrons.

[8] The LDA/FLAPW calculations also allow one to deduce effective masses for a particular orbit. As might be expected, it is found that the experimentally-observed de Haas–van Alphen frequencies shown in figure 5(a) in general correspond to the calculated orbits with the lowest effective masses.

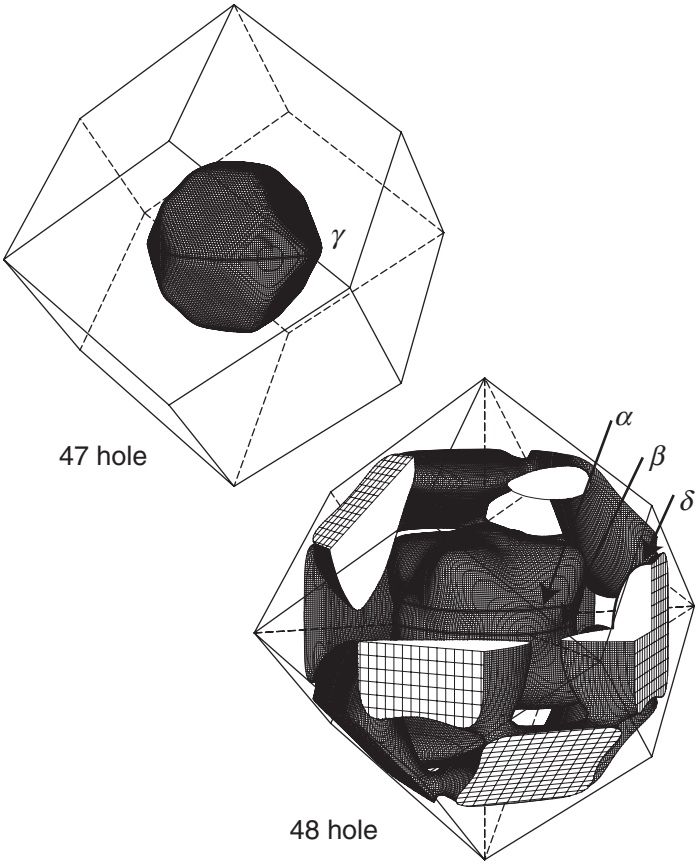

Figure 4. Predicted Fermi surface of $PrOs_4As_{12}$, using the LDA/FLAPW calculation of $LaOs_4As_{12}$ on the $PrOs_4As_{12}$ lattice. For clarity, the 47th and 48th hole-band FSSs are shown separately. The bold lines represent the extremal orbits corresponding to the four main de Haas–van Alphen frequencies, α, β, γ and δ. The three former orbits are illustrated for a vertical applied field; to aid visibility, the δ orbit is shown for a horizontal field.

4.3. Quasiparticle effective masses

Effective masses are derived from the de Haas–van Alphen oscillations by fitting the temperature-dependent Fourier amplitude $A(T)$ to the relevant part of the three-dimensional Lifshitz–Kosevich formula [21]

$$A(T) \propto \frac{\chi}{\sinh \chi}, \tag{1}$$

where $\chi = 14.69\, m^* T/B$, with m^* the quasiparticle cyclotron effective mass and B the reciprocal of the mean inverse field of the window used for the Fourier transform.

First, the effective masses corresponding to spin-up and spin-down components of each de Haas–van Alphen frequency in $PrOs_4As_{12}$ were evaluated independently, using a wide Fourier window to ensure that the two separate components were resolved (see figure 3(c)). Within experimental errors, the effective masses of the spin-up and spin-down components of each frequency were found to be identical.

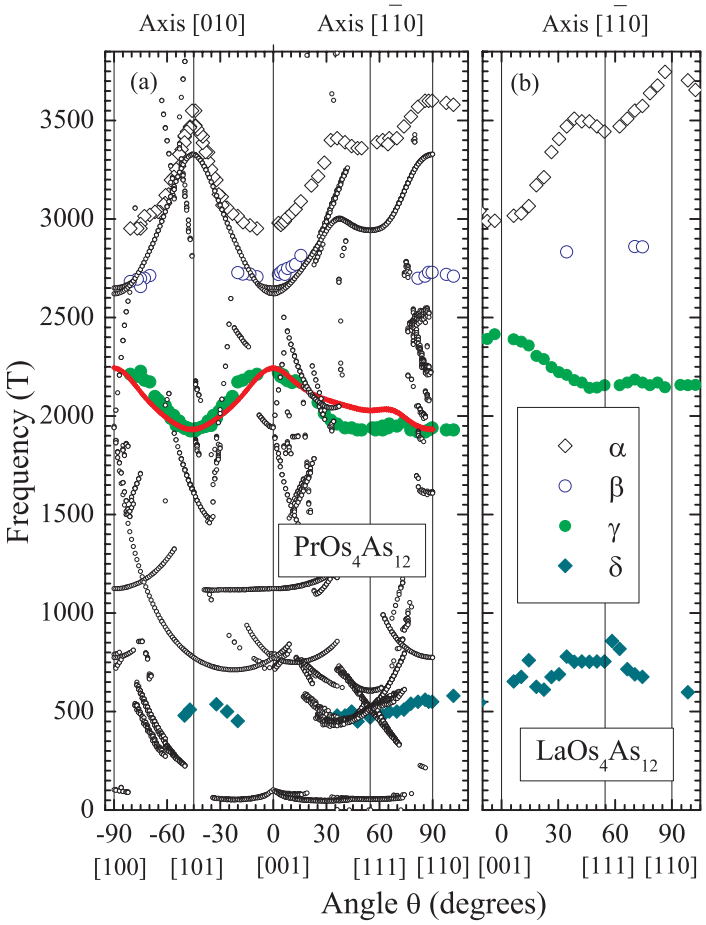

Figure 5. (a) $PrOs_4As_{12}$ de Haas–van Alphen frequencies (PMM phase) as a function of field orientation for rotation of the sample about the [1$\bar{1}$0] axis (positive θ values) and [010] axis (negative θ values). Angles for which the magnetic field lies along crystal axes are indicated by vertical lines. Curves formed from smaller points denote the theoretical frequencies for the 47th (red solid curve) and 48th (hollow points) hole-band Fermi surfaces shown in figure 4. (b) $LaOs_4As_{12}$ de Haas–van Alphen frequencies as a function of field orientation for rotation of the sample about the [1$\bar{1}$0] axis. In both (a) and (b), the absence of a symbol at a particular angle indicates that that frequency could not be observed or was indistinct. The inset key indicates the labeling of the FSSs.

The fact that both spin-up and spin-down components have very similar masses is an important consideration in the investigation of the field dependence of the effective masses in $PrOs_4As_{12}$ described in the following paragraphs. Such a study necessitates the use of a narrower field window (and thus lower frequency resolution); hence, it is not possible to resolve the separate spin-up and spin-down components of each FSS. The masses evaluated are therefore the average effective masses of the spin-up and spin-down components of each FSS.

To investigate the field dependence of the effective masses, de Haas–van Alphen oscillations were recorded at several fixed temperatures in the range 0.45–3.0 K. For each data set, Fourier transforms were performed over a restricted window of inverse magnetic field

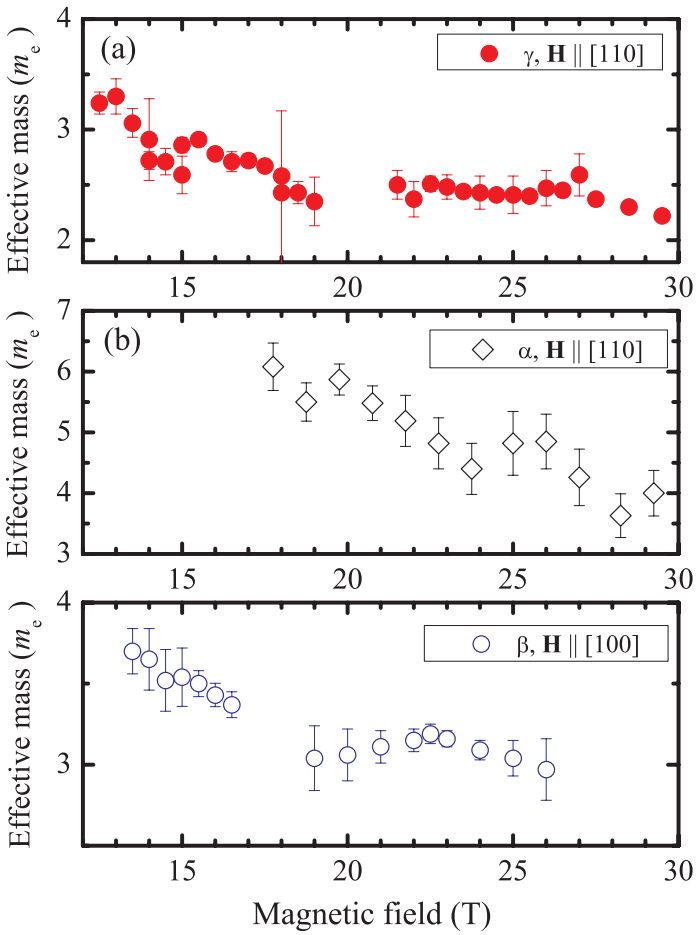

Figure 6. Examples of field-dependent effective masses of $PrOs_4As_{12}$ (PMM phase) derived from the temperature dependence of the de Haas–van Alphen oscillations (equation (1)). The magnetic field plotted is the reciprocal of the mean inverse field of the Fourier-transform window; typically, the window width used was in the range 0.005–0.011 T^{-1}. (a) γ FSS, **H** || [110]. (b) α FSS, **H** || [110]. (c) β FSS, **H** || [100]. Note that gaps in the data correspond to nodes in the de Haas–van Alphen oscillations caused by the beating of the spin-up and spin-down components (see figures 3(c) and (d)).

(typical window width 0.005–0.011 T^{-1}), and the temperature-dependent amplitude fitted to equation 1. Typical mass data are shown in figure 6. Within the errors of the experiment, the masses *decrease* with *increasing* magnetic field; this field-induced change in the mass becomes more noticeable below $\mu_0 H = 20$ T.

The possibility of magnetic-field dependent effective masses in strongly-correlated electron systems has been discussed by a number of authors [24]–[26]. For instance, Schotte and Schotte [26] use a Kondo-impurity model that invokes a narrow resonance (width $\sim k_B T_K$, where T_K is the Kondo temperature) in the density of states at the chemical potential that undergoes Zeeman splitting in a magnetic field. Though this approach is only strictly applicable to dilute alloys such as $La_{1-x}Ce_xB_6$ ($x \ll 1$ [27]), it should be noted that it can provide a

phenomenological description of the heat capacity $C(H,T)$ of the paramagnetic phase of $PrOs_4As_{12}$ for $\mu_0 H \lesssim 16\,\mathrm{T}$ and $0.4 \lesssim T \lesssim 12\,\mathrm{K}$ [13]. The model predicts a strong decrease in the electronic specific heat coefficient γ (and, consequently, the average quasiparticle effective mass) with magnetic field, yielding a small Kondo temperature $T_\mathrm{K} \sim 3.5\,\mathrm{K}$. This is similar to the value $T_\mathrm{K} \sim 1\,\mathrm{K}$ obtained from a scaling analysis of the electrical resistivity $\rho(H,T)$ as a function of H and T [13]. The scaling analysis was based on a calculation due to Schlottmann [28], also for the Kondo impurity case. The two models applied to the $C(H,T)$ and $\rho(H,T)$ data for $PrOs_4As_{12}$ in the paramagnetic phase, were for the case of spin $S = 1$, which is appropriate for a triplet ground state (Γ_5) for $PrOs_4As_{12}$ in the CEF [12, 13].

In spite of this qualitative success of the Kondo impurity models, the Anderson lattice models used to treat itinerant heavy-fermion metals [24, 25] might be expected to be more relevant to $PrOs_4As_{12}$. However, the authors of [24, 25] suggest very different behavior for the spin-up and spin-down components of each FSS, a prediction that was backed up at least qualitatively by the experiments on pure CeB_6 [29] and $CePd_2Si_2$ [30]. In $CePd_2Si_2$, differing, field-dependent masses are inferred for the two spin components of the Fermi surface [30]. However, in CeB_6, a field-dependent mass is observed for the minority-spin FSS while the de Haas–van Alphen oscillations for the majority-spin Fermi surface are not observed, because of a very heavy mass and/or spin-dependent scattering [31, 32]. (It should be noted that the situation in $Ce_xLa_{1-x}B_6$ with large Ce concentrations is less clear cut, with some studies reporting only one spin component in the de Haas–van Alphen oscillations [31, 32], while others infer the presence of spin-up and spin-down FSSs from detailed analysis of the temperature dependence or phase of the oscillations [27, 33].)

By contrast with the predictions of [24, 25], both spin-up and spin-down components are observed for all FSSs of $PrOs_4As_{12}$, and their behavior with changing field (e.g. the values of their effective masses) appears identical. It is therefore unlikely that the Anderson lattice models [24, 25] are applicable to $PrOs_4As_{12}$. Instead, the enhancement of the effective mass in the PMM phase of $PrOs_4As_{12}$ is most likely to be due to fluctuations associated with the proximity of the antiferromagnetic phase. As one moves away from this phase in magnetic field, the fluctuations will be gradually suppressed, leading to quasiparticle masses that gradually decrease (figure 6). The gradual reduction in the electronic contribution to the heat capacity with increasing field in the PMM phase referred to above [13] is likely to be due to the same mechanism.

Some illustrative values of the effective masses in $PrOs_4As_{12}$ for the various FSSs, evaluated at a field of 25 T, are shown in table 1. By contrast, the behavior of $LaOs_4As_{12}$ is more conventional, in that the masses are relatively small compared to those in $PrOs_4As_{12}$, and field-independent; a summary is given in table 2 (cf the comparison of $PrOs_4Sb_{12}$ and $LaOs_4Sb_{12}$ given in [8]). Effective masses associated with various Fermi-surface orbits may also be deduced from the LDA/FLAPW calculations (the identification of the orbits involved is covered in sections 4.1 and 4.2); theoretical values are compared with experimental data in table 3. The fluctuations discussed above lead to experimental masses at 25 T that are enhanced by a factor $\sim$3–5 with respect to the bandstructure calculations.

The high-field paramagnetic state corresponds to a field-induced ferromagnetic state. As noted above, the de Haas–van Alphen branches are thus split into separate frequencies corresponding to spin-up and spin-down quasiparticles by the ferromagnetic exchange interactions. To quantify this splitting, the effective masses can be used to estimate the

Table 1. Selected Fermi-surface properties of $PrOs_4As_{12}$ in its PMM phase. The first column denotes the FSS, and the second the field orientation; $\langle F \rangle$ is the mean of the separate spin-up and spin-down frequencies, and ΔF is their difference, evaluated at $\mu_0 H = 25\,\mathrm{T}$. The effective masses are also evaluated at 25 T, using a Fourier window of width $0.011\,\mathrm{T}^{-1}$. The final column is the estimated direct exchange energy calculated using the tabulated parameters.

FSS	Orientation	$\langle F \rangle$ (T)	ΔF (T)	$m^*(m_e)$	E_{exch} (meV)
γ	$\mathbf{H} \parallel [100]$	2210 ± 10	50	2.6 ± 0.2	1.1
β	$\mathbf{H} \parallel [100]$	2740 ± 10	75	3.0 ± 0.1	1.4
α	$\mathbf{H} \parallel [100]$	3005 ± 10	60	4.4 ± 0.1	0.8
γ	$\mathbf{H} \parallel [110]$	1926 ± 10	40	2.4 ± 0.2	1.0
α	$\mathbf{H} \parallel [110]$	3510 ± 10	60	4.8 ± 0.3	0.7
γ	$\mathbf{H} \parallel [111]$	2028 ± 10	50	2.7 ± 0.4	1.1

Table 2. Selected Fermi-surface properties of $LaOs_4As_{12}$. The first column denotes the FSS, and the second the field orientation; F is the de Haas–van Alphen frequency. The effective masses, which are field-independent, are evaluated at 13.6 T.

FSS	Orientation	F(T)	$m^*(m_e)$
γ	$\mathbf{H} \parallel [100]$	2425 ± 10	1.31 ± 0.08
α	$\mathbf{H} \parallel [100]$	3045 ± 10	2.0 ± 0.1
γ	$\mathbf{H} \parallel [110]$	2182 ± 10	1.12 ± 0.04
α	$\mathbf{H} \parallel [110]$	3770 ± 10	3.3 ± 0.5
γ	$\mathbf{H} \parallel [111]$	2185 ± 10	1.14 ± 0.05
α	$\mathbf{H} \parallel [111]$	3525 ± 10	2.8 ± 0.2

direct exchange energy in $PrOs_4As_{12}$ by comparing effective Fermi energies for the spin-up and spin-down components. For a particular de Haas–van Alphen frequency F, with associated effective mass m^*, the effective Fermi energy is heF/m^*. The direct exchange energy E_{exch} is one half of the difference between effective Fermi energies for the spin-up and spin-down components [23]:

$$E_{exch} = \frac{\hbar \Delta F}{2m^*}, \tag{2}$$

where ΔF is the difference in de Haas–van Alphen frequency. Some illustrative values of E_{exch} are listed in table 1; all are close to 1 meV, and similar in magnitude to the exchange energies observed in the 4f hexaborides (see [23] and citations therein).

5. Discussion

Given the valences of La and Pr, the similarity of the Fermi surfaces of $PrOs_4As_{12}$ and $LaOs_4As_{12}$ suggest that the 4f-electrons of the Pr ions make little contribution to the itinerant

Table 3. Experimental (subscript 'expt'; PMM phase) and theoretical (subscript 'theory') de Haas–van Alphen frequencies F and effective masses m^* for $PrOs_4As_{12}$. The experimental masses were evaluated at 25 T; see table 1.

FSS	F_{expt}(T)	F_{theory}(T)	$\left\lvert\frac{m^*_{\text{expt}}}{m_e}\right\rvert$	$\frac{m^*_{\text{theory}}}{m_e}$	$\left\lvert\frac{m^*_{\text{expt}}}{m^*_{\text{theory}}}\right\rvert$
H ∥ [100]					
γ	2210	2245	2.6 ± 0.2	-0.86	3.0
β	2740	2621	3.0 ± 0.1	-0.87	3.4
α	3005	2651	4.4 ± 0.1	-0.95	4.6
H ∥ [110]					
δ	550	775	–	-1.47	–
γ	1926	1932	2.4 ± 0.2	-0.61	3.9
α	3510	3329	4.8 ± 0.3	-1.60	3.0
H ∥ [111]					
γ	1932	2028	2.7 ± 0.4	-0.60	4.5

quasiparticles in the high-field PMM phase of $PrOs_4As_{12}$. This view is also supported by the strong qualitative similarity between the theoretical de Haas–van Alphen frequencies and the experimental data (figure 5(a)); the LDA/FLAPW calculations assume localized 4f-electrons.

The situation in $PrOs_4As_{12}$ may be rather analogous to that observed in a number of other f-electron systems (see [34] and citations therein). It is likely that both the antiferromagnetic and PMM phases possess highly-correlated 4f electrons, but with somewhat different effective Kondo temperatures. In such a scheme, the effective Kondo temperature of the PMM phase will be relatively small (see the values $T_K \sim 1$–3.5 K discussed above [13]), so that the properties of the 4f electrons will be almost indistinguishable from those of localized ionic moments. By comparison, it is likely that the antiferromagnetic metal phase will have a relatively large effective Kondo temperature by comparison, causing the 4f electrons to be in the mixed-valence regime with significant spd and f hybridization at low temperatures. Consequently one might expect the charge degrees of freedom of $PrOs_4As_{12}$ in the antiferromagnetic phase to be describable in terms of itinerant quasiparticles with a large effective mass, a view that is supported by the substantial electronic contribution to the heat capacity [13]. Itinerant quasiparticles are preferable from a zero-point energy standpoint at low temperatures, but the quasi-localized 4f electrons of the PMM phase will be favored on entropic grounds at elevated temperatures and fields [34]. Although the exact details may differ, a similar picture was recently found to obtain in $CeIn_3$ [35]. Here, Fermi-surface pockets of very heavy quasiparticles are observed in the antiferromagnetic phase at low magnetic fields [35]. The presence of these itinerant quasiparticles is able to account for the large value of the electronic heat capacity coefficient γ in the antiferromagnetic phase. However, as the field is increased, the heavy-quasiparticle pockets are destroyed, shortly before the field-induced suppression of antiferromagnetism.

6. Summary

The susceptibility and de Haas–van Alphen effect have been measured in single crystals of the filled skutterudites $PrOs_4As_{12}$ and $LaOs_4As_{12}$ using both pulsed and quasistatic magnetic fields. A cascade of three or four strongly field-orientation-dependent metamagnetic transitions is observed in $PrOs_4As_{12}$ on sweeping the field from the antiferromagnetic phase to the PMM phase. The Fermi-surface topologies of $LaOs_4As_{12}$ and the PMM phase of $PrOs_4As_{12}$ are found to be very similar. In addition, they are in reasonable agreement with the predictions of bandstructure calculations for $LaOs_4As_{12}$ on a $PrOs_4As_{12}$ lattice. Both facts suggest that the 4f electrons of Pr are essentially localized in the PMM phase of $PrOs_4As_{12}$. However, while the properties of $LaOs_4As_{12}$ suggest a conventional nonmagnetic Fermi liquid, the effects of direct exchange and electron correlations may be detected in the PMM phase of $PrOs_4As_{12}$; a direct exchange energy ≈ 1 meV splits the bands, leading to beats in the de Haas–van Alphen oscillations, and the quasiparticle effective masses in $PrOs_4As_{12}$ are found to decrease with increasing field, probably reflecting the gradual suppression of magnetic fluctuations associated with proximity to the low-temperature, low-field antiferromagnetic state.

Acknowledgments

Research at UCSD was supported by the US Department of Energy (DoE) under grant no DE-FG02-04ER46105, the US National Science Foundation (NSF) under grant no DMR 0335173, and the National Nuclear Security Administration under the Stewardship Science Academic Alliances Program through DOE Research grant no DE-FG52-03NA00068. The work carried out at NHMFL was supported by DoE (grant LDRD-DR 20070013) and by NSF and the State of Florida. Studies at Kobe are supported by a Grant-in-Aid for Scientific Research Priority Area 'Skutterudite' (15072204), MEXT, Japan. We thank Neil Harrison, Ross McDonald and Stan Tozer for experimental assistance and useful discussions.

References

[1] Aoki Y, Sugawara H, Harima H and Sato H 2005 *J. Phys. Soc. Japan* **74** 209
[2] Maple M B, Bauer E D, Frederick N A, Ho P-C, Yuhasz W A and Zapf V S 2003 *Physica* B **328** 29
[3] Meisner G P, Torikachvili M S, Yang K N, Maple M B and Guertin R P 1985 *J. Appl. Phys.* **57** 3073
[4] Kuric M V, Guertin R P, Torikachvili M S, Maple M B and Foner S 1990 *J. Appl. Phys.* **67** 4818
[5] Aoki Y, Higemoto W, Sanada S, Ohishi K, Saha S R, Koda A, Nishiyama K, Kadono R, Sugawara H and Sato H 2005 *Physica* B **359–61** 895
[6] Maple M B, Ho P-C, Zapf V S, Frederick N A, Bauer E D, Yuhasz W M, Woodward M and Lynn J W 2002 *J. Phys. Soc. Japan* **71** (suppl.) 23
[7] Sugawara H, Matsuda T D, Abe K, Aoki Y, Sato H, Nojiri S, Inada Y, Settai R and Onuki Y 2002 *Phys. Rev.* B **66** 134411
[8] Sugawara H *et al Phys. Rev.* B **66** 220504
[9] Maple M B, Henkie Z, Yuhasz W M, Ho P-C, Yanagisawa T, Sayles T A, Butch N P, Jeffries J R and Pietraszko A 2007 *Proc. Int. Conf. on Magnetism* (*Kyoto*) *J. Magn. Magn. Mater.* **310** 182
[10] Maple M B, Ho P-C, Zapf V S, Yuhasz W M, Frederick N A and Bauer E D 2003 *Physica* C **388–9** 549
[11] Sugawara H, Kobayashi M, Osaki S, Saha S R, Namiki T, Aoki Y and Sato H 2005 *Phys. Rev.* B **72** 014519
[12] Yuhasz W M *et al* 2006 *Phys. Rev.* B **73** 144409
[13] Maple M B *et al* 2006 *Proc. Natl. Acad. Sci. USA* **103** 6783

[14] Brooks J S, Naughton M J, Ma Y P, Chaikin P M and Chamberlain R V 1987 *Rev. Sci. Instrum.* **58** 117
[15] Harrison N, House A, Deckers I, Caulfield J, Singleton J, Herlach F, Hayes W, Kurmoo M and Day P 1995 *Phys. Rev.* B **52** 5584
[16] Singleton J, Mielke C H, Migliori A, Boebinger G S and Lacerda A H 2004 *Physica* B **346–7** 614
[17] Harima H 2001 *J. Magn. Magn. Mater.* **48–50** 83
[18] Harima H and Takegahara K 2002 *Physica* B **312–3** 843
[19] Goddard P A, Singleton J, Lima-Sharma A L, Morosan E, Blundell S J, Bud'ko S L and Canfield P C 2007 *Phys. Rev.* B **75** 094426
[20] Shirotani I, Ohno K, Sekhine C, Yagi T, Kawakami T, Nakanishi T, Takahashi H, Tang J, Matsushita S and Matsumoto T 2000 *Physica* B **281–2** 1021
[21] Shoenberg D 1984 *Magnetic Oscillations in Metals* (Cambridge: Cambridge University Press)
[22] Sugawara H, Abe Y, Aoki Y, Hedo M, Settai R, Onuki Y and Harima H 2000 *J. Phys. Soc. Japan* **69** 2938
[23] Goodrich R G, Harrison N and Fisk Z 2006 *Phys. Rev. Lett.* **97** 146404
[24] Wasserman A and Springford M 1996 *Adv. Phys.* **45** 471
Wasserman A, Springford M and Hewson A C 1989 *J. Phys.: Condens. Matter* **1** 2669
[25] Edwards D M and Green A C M 1997 *Z. Phys.* B **103** 243
[26] Schotte K D and Schotte U 1975 *Phys. Lett.* A **55** 38
[27] Mihut I, Migliori A, Singleton J, Gor'kov L, Pham L, Capan C and Fisk Z 2007 in preparation
[28] Schlottmann P 1983 *Z. Phys.* B **51** 223
[29] Harrison N, Meeson P, Probst P-A and Springford M 1993 *J. Phys.: Condens. Matter* **5** 7435
[30] Sheikin I, Gröger A, Raymod S, Jaccard D, Aoki D, Harima H and Flouquet J 2003 *Phys. Rev.* B **67** 094420
[31] Goodrich R G, Harrison N, Teklu A, Young D and Fisk Z 1999 *Phys. Rev. Lett.* **82** 3669
[32] Teklu A A, Goodrich R G, Harrison N, Hall D, Fisk Z and Young D 2000 *Phys. Rev.* B **62** 12875
[33] Endo M, Nakamura S, Isshiki T, Kimura N, Nojima T, Aoki H, Harima H and Kunii S 2006 *J. Phys. Soc. Japan* **75** 114704
[34] Drymiotis F, Singleton J, Harrison N, Lashley J C, Bangura A, Mielke C H, Balicas L, Fisk Z, Migliori A and Smith J L 2005 *J. Phys.: Condens. Matter* **17** L77
[35] Sebastian S E, Harrison N, Batista C D, Trugman S A, Fanelli V, Jaime M, Murphy T P, Palm E C, Harima H and Ebihara T 2007 in preparation